Consiglio Nazionale delle Ricerche
National Research Council of Italy

Istituto di Geoscienze e Georisorse
Institute of Geosciences and Earth Resources

SegemAR
Servicio Geológico
Minero Argentino

SOCOMPA GEOTHERMAL PROSPECT
Report on fluid geochemistry
(Soil CO_2 degassing)

Elaborated by:
Dr. Brunella Raco

Institute of Geosciences and Earth Resource (IGG)
National Research Council (CNR-Italy)

September 2018

1 Introduction

The Servicio Geológico Minero Argentino (SEGEMAR), in collaboration with the Institute of Geoscience and Earth Resources of the National Research Council of Italy (IGG-CNR) have carried out, during April 2018, a CO_2 flux survey in the Socompa Volcano area.

The accumulation chamber method has been used to measure the CO_2 flux diffuse at the air-soil interface. Data processing have been performed throughout statistical and geostatistical analysis aimed at evaluating the statistical distribution of the data set and the presence of anomalous data.

This report shows the methodology used and the main results obtained.

2 Methods

The Fluxmeter used is a portable instrument for the measurement of soil diffuse flux of gases applying the accumulation chamber method. This method is widely used for quantifying soil respiration in agronomy (e.g., Parkinson, 1981) and soil degassing in volcanic areas (e.g., Chiodini et al., 1998). It has been implemented by West Systems and it allows to take measurements of very high accuracy in a short time, covering large ranges of CO_2 and CH_4 diffuse fluxes from soil.

The instrument consists of 4 principal parts (Figure 1):

1. One accumulation chamber.
2. A carbon dioxide detector.
3. A methane detector.
4. A palmtop computer with integrated GPS.

The specifications of each component are illustrated below. Furthermore, Table 1 displays the flux range (in mol m^{-2} d^{-1}) for each gas, as well as the *low detection limit* (LDL) and the full scale (FS).

WS-LI820: Carbon dioxide detector. The West Systems Fluxmeter is equipped with a LICOR LI-820 carbon dioxide detector, whose specifications are as follows: Double beam infrared sensor compensated for temperature variations in the range of -10 to 45°C and for atmospheric pressure variations in the range of 660-1060 HPa. Concentration measurement range: 0-20,000 ppmv.

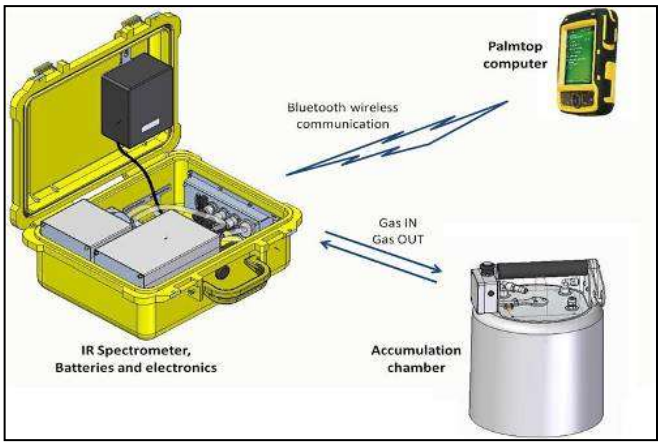

Figure 1. Framework of west Systems Fluxmeter.

Global positioning system receiver. The WS-GPS embedded in the palmtop, allows the Geo-referencing of each measurement station. During the flux measurement the position/elevation data are recorded by the flux-manager software and a "mean" position of the measured point is computed in order to reduce the GPS position-fix error. The precision depends on sky-view and on satellites costellation at measurement time. The position data are reported in latitude/longitude degrees (geodetic datum WGS84) and after a PC-based post processing (Flux Revision) also in UTM coordinates. The elevation is reported in meters above sea level.

Warm Up. Only at instrument cold start-up a warm-up time of 20 minutes is required. The typical measurement time ranges from 2 to 4 minutes and the autonomy of the instrument is about 4 hours with a single NiMH 14.4 Volts, 4.5 A/h battery. The instrument comes with two interchangeable batteries.

Accumulation Chamber specifications. The instrument comes with one accumulation chamber with diameter 200 mm, height 100 mm and weight: 1.5 kg.

Palmtop computer. Palmtop based on Windows Mobile (or optionally ANDROID) operating system; integrated GPS, touchscreen, wireless communication with fluxmeter (via Bluetooth).

Table 1. Flux Range for CO_2 fluxes.

Gas	**Methodology**	**LDL**	**FS**
		10^{-3}·[mol $m^{-2}d^{-1}$]	**[mol $m^{-2}d^{-1}$]**
CO_2	IR Spectrometry	2	300

2.1 Adopted methods of data processing

Data processing consists in a first statistical analysis aimed at evaluating the statistical distribution of the data set. Two different software codes, ProUCL and Statistica 7, were used to investigate the frequency distribution of CO_2 fluxes. These software codes were also employed to evaluate the main statistical parameters of the measured gas and to process the data in order to build histograms, box plots and quantile-quantile plots (Q-Q plots).

CO_2 flux data were partitioned following the approach of Sinclair (1974, 1991). Main statistical parameters were computed for each individual population, including the Arithmetic Mean of Raw Data (AMRD) and the 95% confidence interval of the mean, which was obtained using the Sichel's t-estimator (Sichel, 1966). Results of partitioning were also used to evaluate the local background threshold of soil CO_2 fluxes. This evaluation was performed by means of the ProUCL software code, following the indication of US-EPA, that is assuming the 95% Upper Tolerance Limit (UTL) of the second higher statistical population as robust indicator of the local background threshold of soil CO_2 fluxes. This value is the maximum soil CO_2 flux expected for bacterial activity in the rhizosphere and soil respiration. Measures exceeding this threshold, that cannot be explained by biogenic soil emissions, were considered as the product of other sources, presumably deep, including geothermal degassing.

Box-Whisker plots and an analytical process based on the Central Limit Theorem (Singh, 1993; Singh et al., 1997) were used to individuate potential outliers. Values lower than the instrumental detection limit (DL, equal to 0.002 mol m^{-2} d^{-1} for CO_2) were eliminated from the

original data set in the data processing. In contrast, potential outliers and values below DL were assumed equal to DL/2 and included in the geostatistical data elaboration.

For what concerns the geostatistical data processing, data were processed using the ISATIS software package that allows the realization of both the experimental variogram and the variogram model. A "cross-validation" test was performed to evaluate the goodness of the selected variogram model (Devijver et al., 1982; Krige, 1951; Matheron, 1962, 1965, 1969, 1970; Matheron and Monget, 1969; David, 1977; Clark, 1979; Chauvet, 1982; Chauvet and Galli, 1982, Armstrong, 1984a, 1984b; Chauvet, 1991, 1993; Wackernagel, 1995).

3. Diffuse soil degassing in the Socompa Volcano area

3.1 Statistical analysis of CO_2 fluxes

The main statistical parameters of the 285 measurements of CO_2 diffuse fluxes from soil carried out in the Socompa Volcano area are shown in Table 2, while their geographical distribution is reported in Figure 2, together with the indication of the investigated areas. Area A indicates the zone surrounding the Socompa Laguna, area B includes the "Quebrada del Agua" spring, area C is located between the two domes situated in the norther part of the Socompa Lagoon and area D at the base of the Socompa Volcano lava flow. These statistical parameters were computed assuming that all the measurements below DL are equal to DL/2, that is 0.001 mol m^{-2} d^{-1}.

Table 2. Descriptive statistics for the CO_2 diffuse fluxes from soil in the Socompa Volcano area

	N	Mean	Median	Minimum	Maximum	Std.Dev.	Coef.Var.	Skewness	Kurtosis
CO_2 [mol m^{-2} d^{-1}]	285	0.034	0.024	0.001	0.217	0.0358	105.1	1.47	2.84

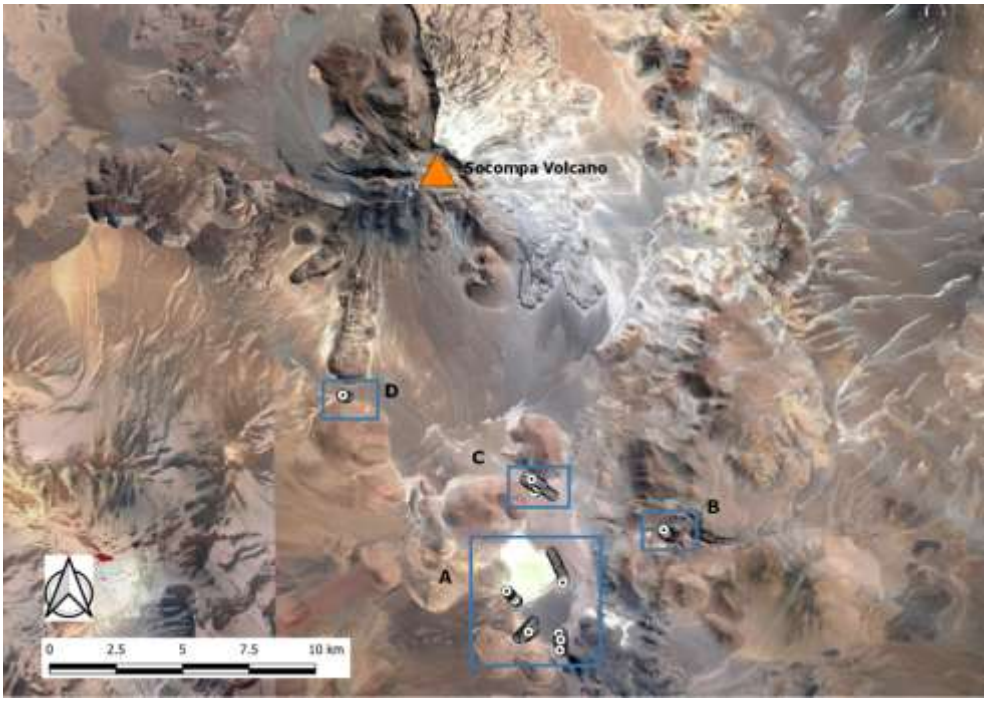

Figure 2. Geographical distribution of CO_2, flux measurements.

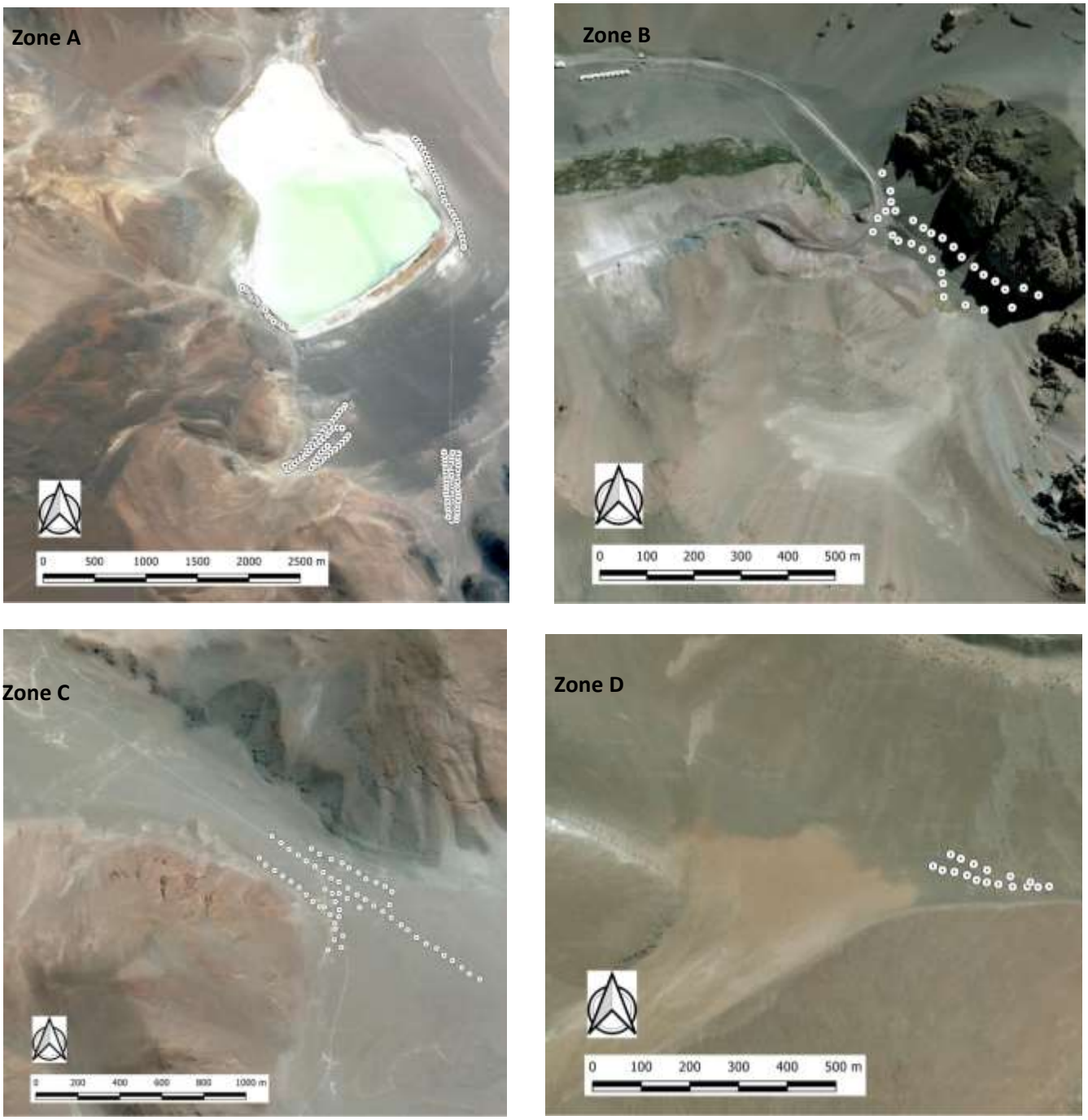

Figure 3. Zoom of each investigated zone.

As shown in Table 3, there are 62 CO_2 fluxes below the DL, indicating that about 22% of the investigated area does not emit measurable carbon dioxide fluxes.

Table 3. Frequency table for the CO_2 fluxes from soil in the Socompa Volcano area. Range in mol m^{-2} d^{-1}.

Range	valid	Cumulate	% Valid	%Cumul
x≤0.002	62	62	21.75	21.75
0.002<x<0.005	14	76	4.91	26.67
0.005≤x<0.01	25	101	8.77	35.44
0.01≤x<0.05	104	205	36.49	71.93
0.05≤x<0.1	64	269	22.46	94.39
x≥0.2	16	285	5.61	100

Excluding data below detection limit (≤0.002 mol m^{-2} d^{-1}), data appears gamma distributed according Kolgromov-Smirnov test. This hypothesis is not confirmed by Anderson-Darling test. For this reason the all dataset has been processed by partitioning procedure. Following the Sinclair's approach, the cumulative curve was partitioned in three individual populations, which are composed by 60, 86 and 77 entries, respectively. The QQ-plot in reported in Figure 4

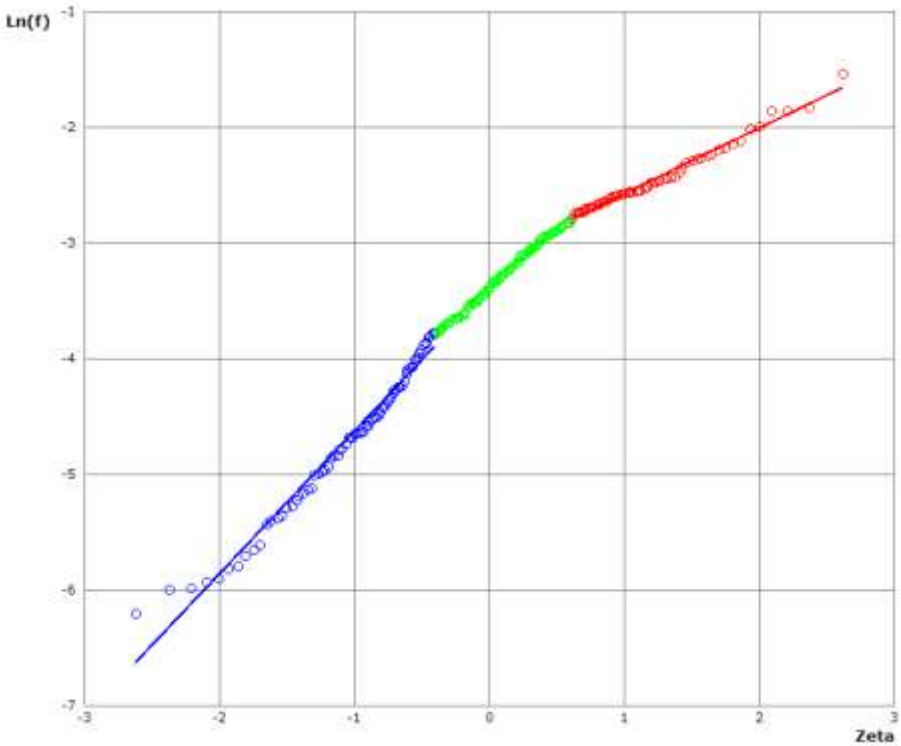

Figure 4 Q-Q plots for the soil fluxes of CO_2 measured in the Socompa Volcano area. The diagram refers to data above detection limit.

The main statistical parameters of these three individual populations are reported in Table 4.

Table 4. Main statistical parameters for the three individual populations of the soil CO_2 flux in the Socompa Volcano area, recognized using the Sinclair's partitioning procedure (values in mol m-2 d-1).

Population	N	Mean	Median	Minimum	Maximum	Variance	Std.Dev.	Coef.Var.	Skewness	Kurtosis
1	60	0.0900	0.0786	0.0620	0.2168	0.00086	0.0293	32.52	2.147	5.603
2	86	0.0395	0.0382	0.0231	0.0616	0.00013	0.0115	29.08	0.293	-1.199
3	77	0.0110	0.0099	0.0020	0.0231	0.00004	0.0060	54.70	0.446	-0.810

The highest population (> 0.0616 mol m^{-2} d^{-1}) was investigated by means of the box plot of Figure 5 to check the presence of potential outliers. Again, the logarithmic scale was adopted on the ordinate axis, as in the Q-Q plot of Figure 4. The box plot of Figure 3.2 suggests that one value (0.217 mol m-2 d-1) is a potential outliers.

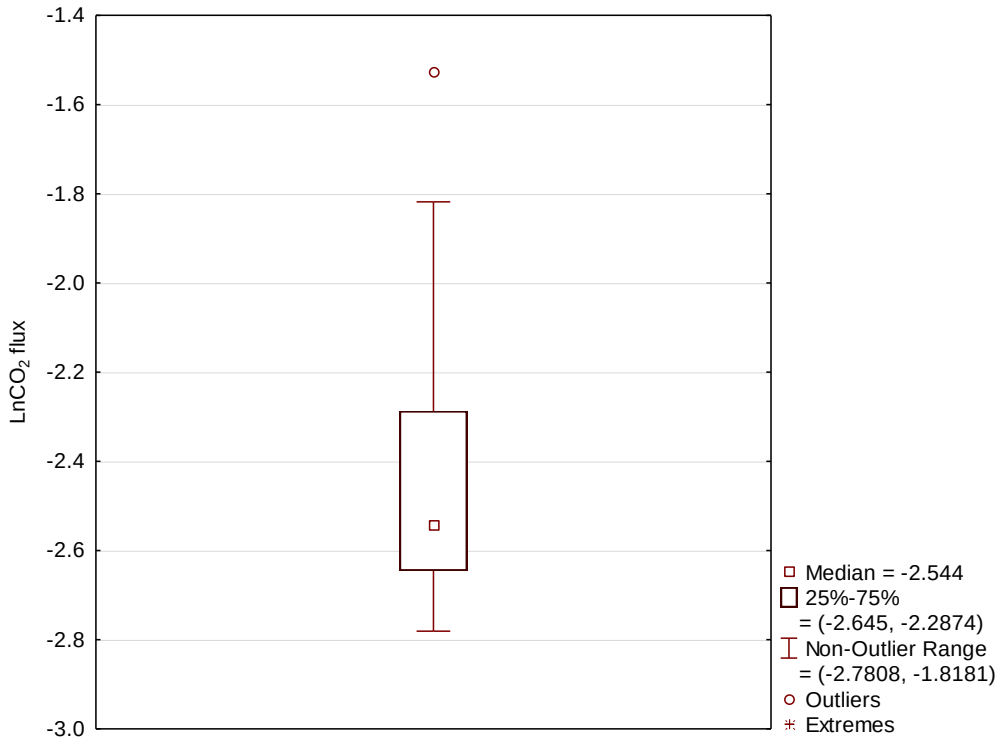

Figure 5. Box plot for population 1 (> 0.0616 mol·m^{-2}·d^{-1}) of soil CO_2 flux in the Socompa Volcano area.

Usually the populations characterized by lower values can be primarily ascribed to natural bacterial activity in the rhizosphere and soil respiration, the observed variability can be related to soils with different vegetation and/or fertility and/or humidity. In almost desert frame such as the investigated area of Socompa volcano this kind of contribution is expected to be much lower than temperate climate zone. Anyway, the presence of micro vegetation mainly represented by vegascan be the origin of the two lower populations 2 (0.0231-0.616 mol·m^{-2}·d^{-1}) and 3 (0.002 – 0.0231 mol·m^{-2}·d^{-1}). The population 1, characterized by higher values (> 0.062 mol·m^{-2}·d^{-1}) should be supported by a different CO_2 source, whose nature could be linked to deep source or to the presence of a more intense radical activity or, again, at different weather conditions.

For what concern weather conditions it worth to mention that data from the weather station of Lullaiaco were processed. The daily trend of air temperature and pressure were for the whole period of the field survey as shown in Figure 12. The air temperature, as showed in the graphics, increased from early morning until the 15:00/16:00 when it started to fall, while the air pressure follows a reverse pattern

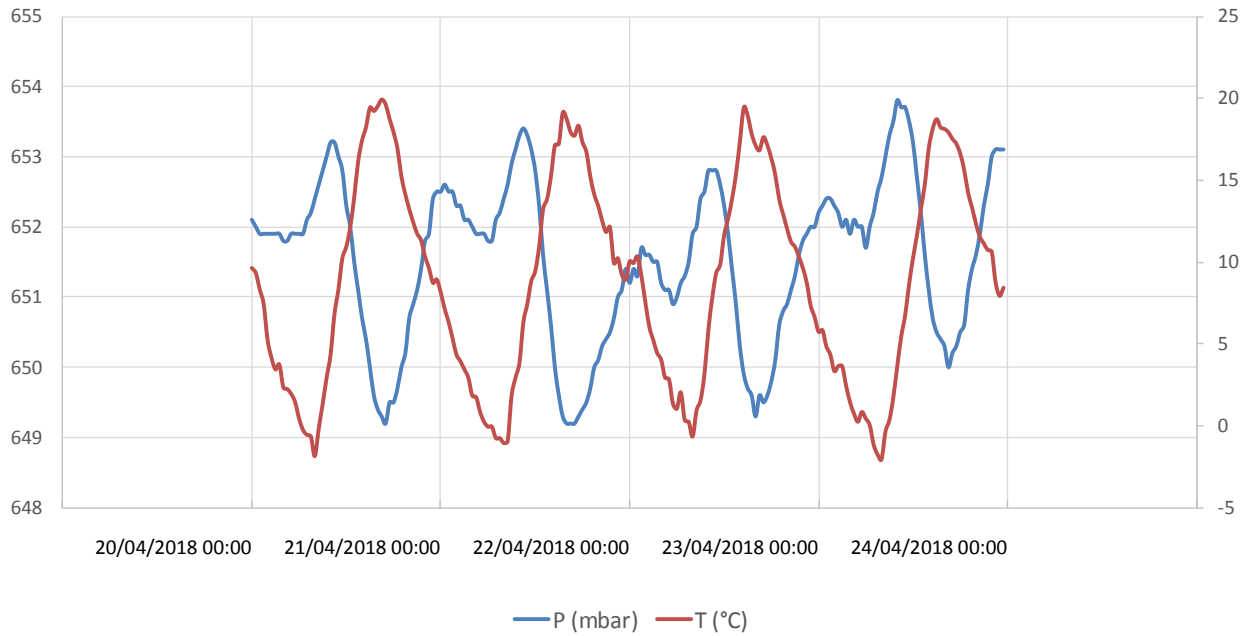

Figure 6. Daily trend of air temperature and pressure at the ….meteorological station

Diffuse soil degassing processes are influenced to varying degrees by the variability of meteorological conditions. Among all the weather parameters, atmospheric pressure, temperature and soil precipitation / humidity, are those that play a major role in the interaction with systems such as the one considered (Pinoult and Baubron, 1996). Physical laws governing degassing processes, clearly show that changes in atmospheric pressure, soil and air temperature, wind speed and soil moisture can cause significant changes in gas flux from soil. The comparison among flux measurements and environmental parameters, in particular, air temperature, air pressure and radiance is shown in Figure 7, Figure 8, Figure 9 and Figure 10, where the trends are separated for each day of the field survey. Inspection of figs 7-10 shows that correlation between the environmental parameters and the flux measurements is rather complex. For example, there are phases of substantial fluctuation of the flux against specific trend of barometric pressure and air temperature, vice versa, periods are observed in which the variations in pressure and /or in temperature correspond to a specific trend of diffuse flux.

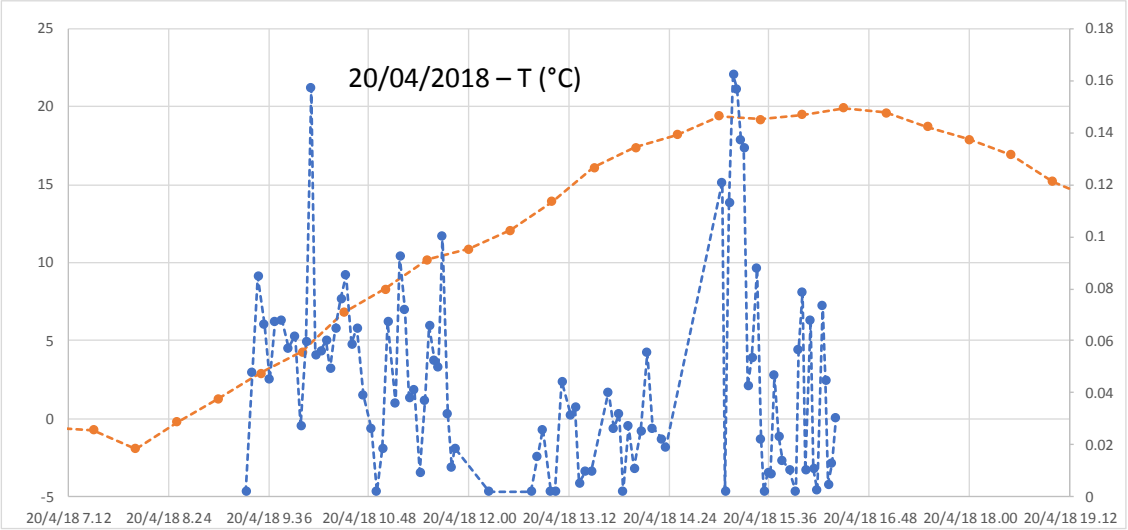
20/04/2018 – T (°C)
25
20
15
10
5
0
-5
0.18
0.16
0.14
0.12
0.1
0.08
0.06
0.04
0.02
0
20/4/18 7.12
20/4/18 8.24
20/4/18 9.36
20/4/18 10.48
20/4/18 12.00
20/4/18 13.12
20/4/18 14.24
20/4/18 15.36
20/4/18 16.48
20/4/18 18.00
20/4/18 19.12

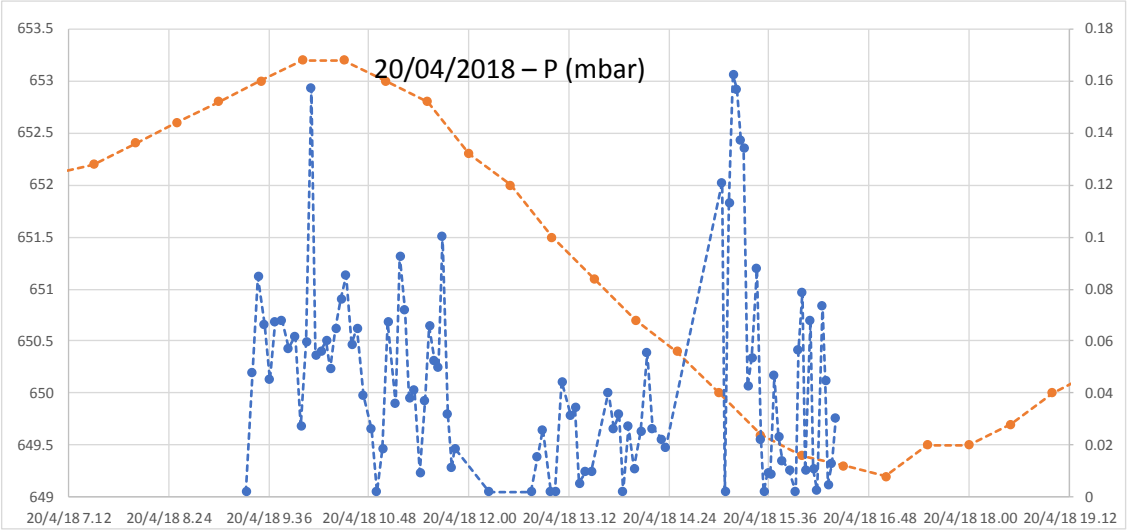
20/04/2018 – P (mbar)
653.5
653
652.5
652
651.5
651
650.5
650
649.5
649
0.18
0.16
0.14
0.12
0.1
0.08
0.06
0.04
0.02
0
20/4/18 7.12
20/4/18 8.24
20/4/18 9.36
20/4/18 10.48
20/4/18 12.00
20/4/18 13.12
20/4/18 14.24
20/4/18 15.36
20/4/18 16.48
20/4/18 18.00
20/4/18 19.12

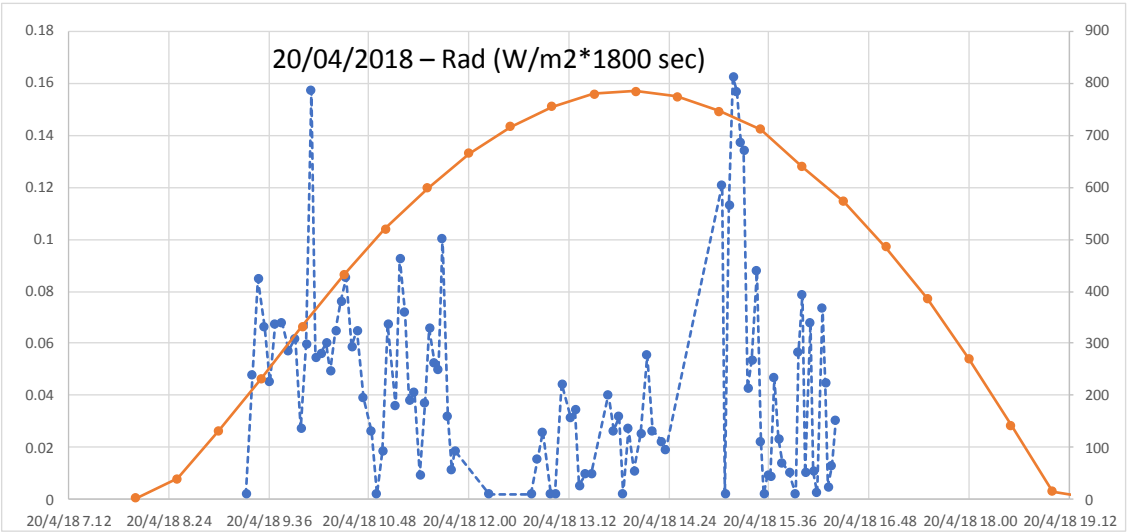
20/04/2018 – Rad (W/m2*1800 sec)
0.18
0.16
0.14
0.12
0.1
0.08
0.06
0.04
0.02
0
900
800
700
600
500
400
300
200
100
0
20/4/18 7.12
20/4/18 8.24
20/4/18 9.36
20/4/18 10.48
20/4/18 12.00
20/4/18 13.12
20/4/18 14.24
20/4/18 15.36
20/4/18 16.48
20/4/18 18.00
20/4/18 19.12

Figure 7. Trend of temperature, pressure and radiance, compared with the flux measurements carried out in 20 April 2018

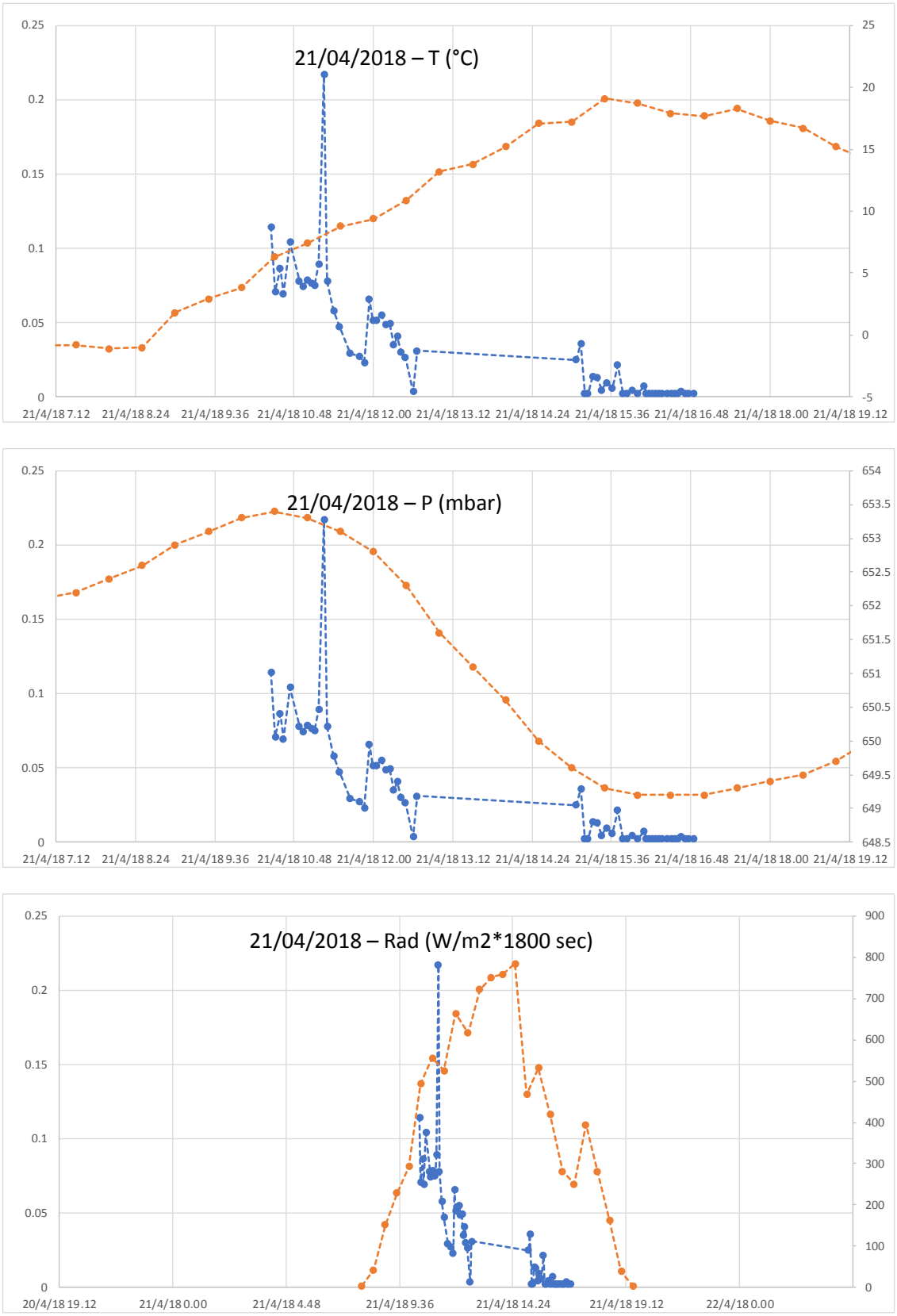

Figure 8. Trend of temperature, pressure and radiance, compared with the flux measurements carried out in 21 April 2018

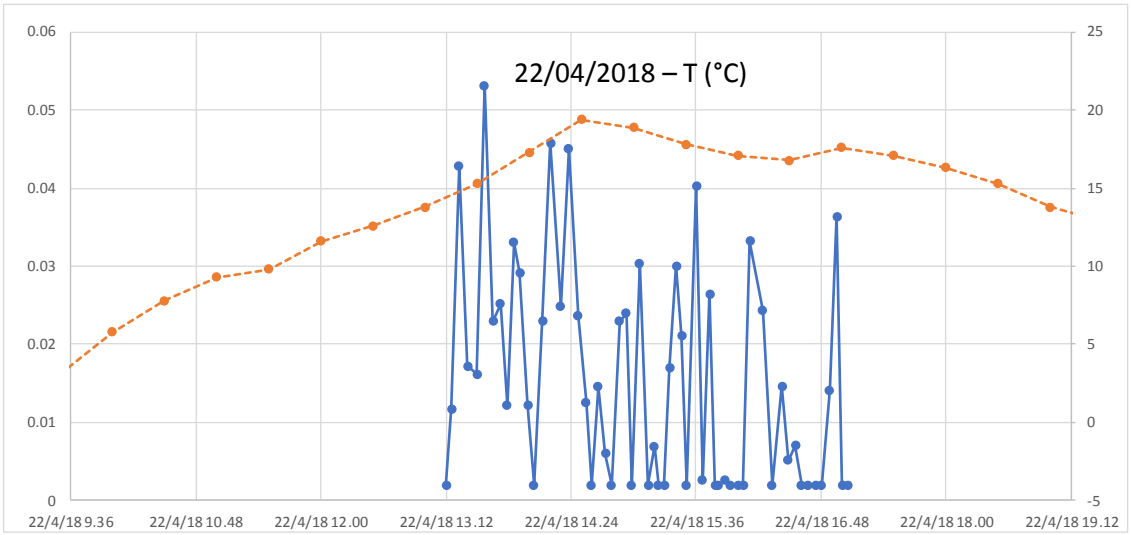

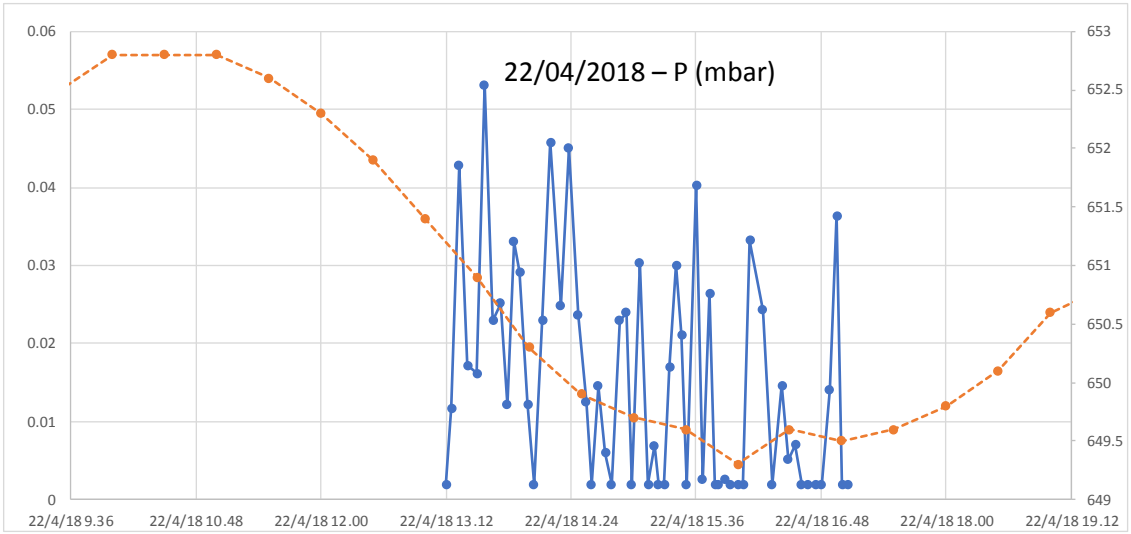

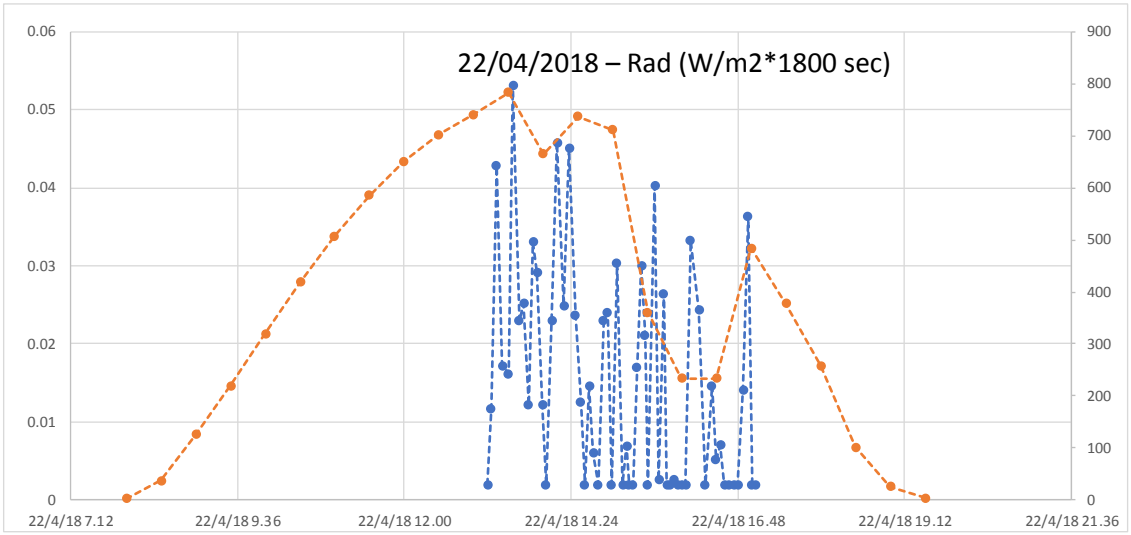

Figure 9. Trend of temperature, pressure and radiance, compared with the flux measurements carried out in 22 April 2018

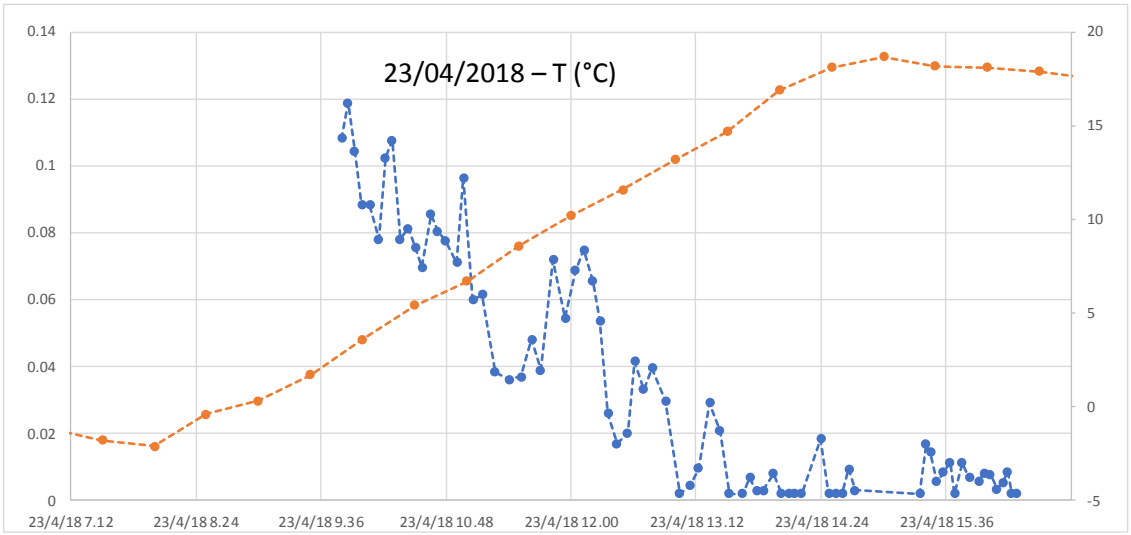

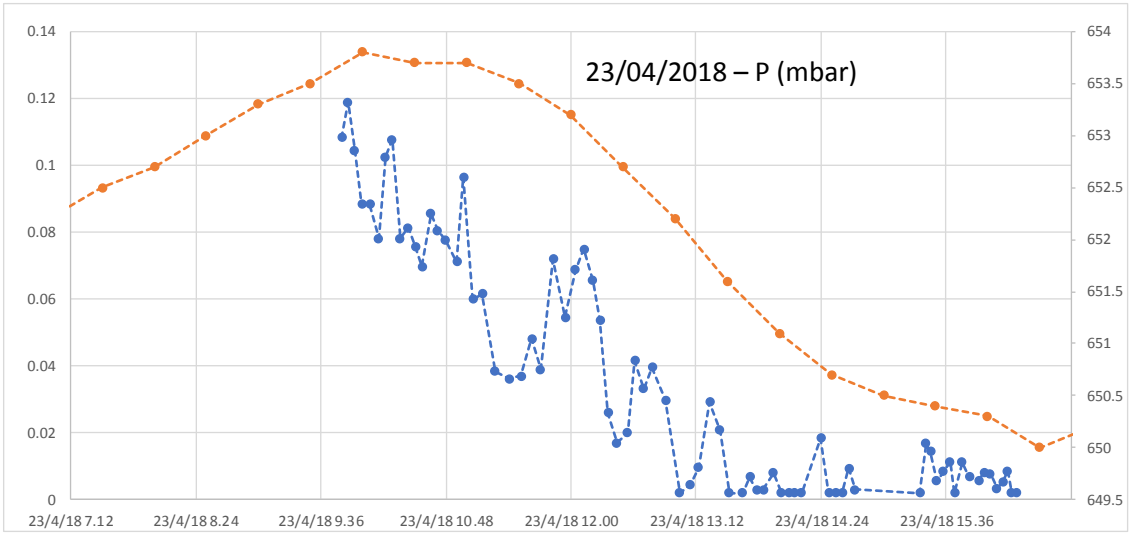

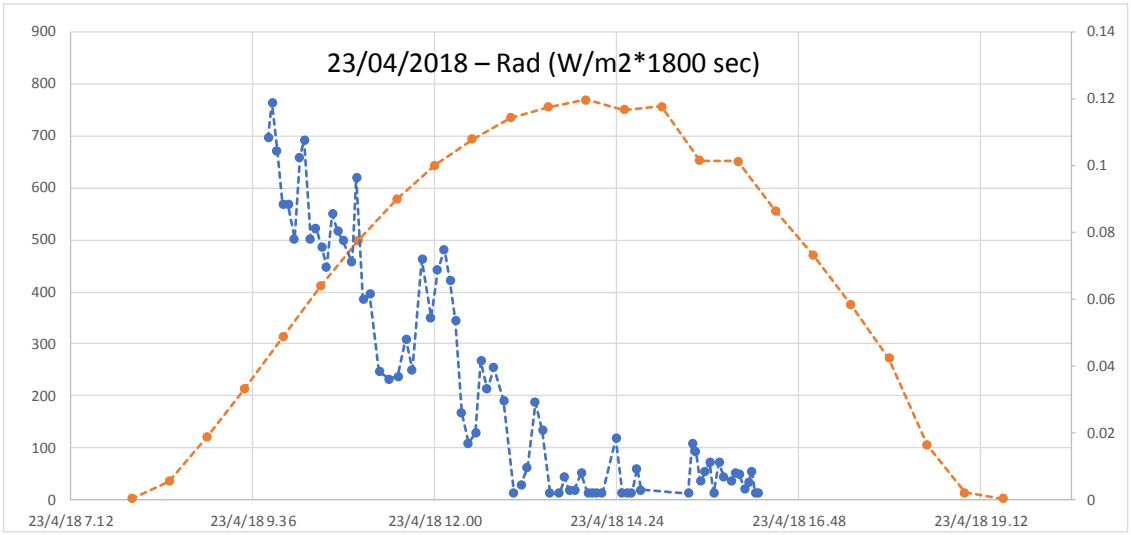

Figure 10. Trend of temperature, pressure and radiance, compared with the flux measurements carried out in 23 April 2018

The identification of which contribution is really acting is not easy without the support of isotopic information. Anyway a deep contribution is normally expected to be visible on a large scale, with connection with geological structures, on the other hands, contribution of bacterial activity can be randomly and discontinuously distributed.

Taking into account populations 2 and 3 the local background threshold of soil CO_2 flux has been evaluated by means of ProUCL software (0.0587 $mol \cdot m^{-2} \cdot d^{-1}$), together with the thresholds among the three recognized populations, were used to elaborate the point map of displaying the spatial distribution of measured CO_2 fluxes. This map shows that the highest values, referring to population 1 (blue points), can be found in A, B and C sub-zones, while there are totally absent in zone D. In sub-zone A there are not values pertaining to population 1 in the eastern border of the Socompa Lagoon and in the south-west zone between the two domes.

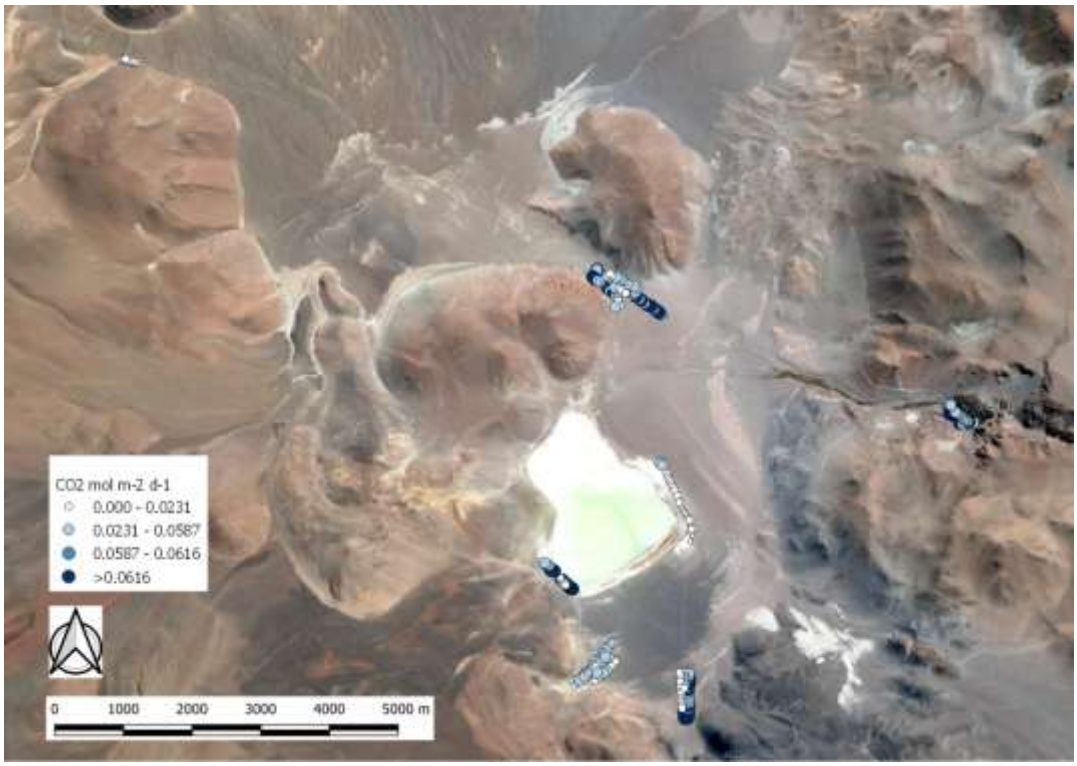

Figure 11a. Geographical distribution of the three different populations.

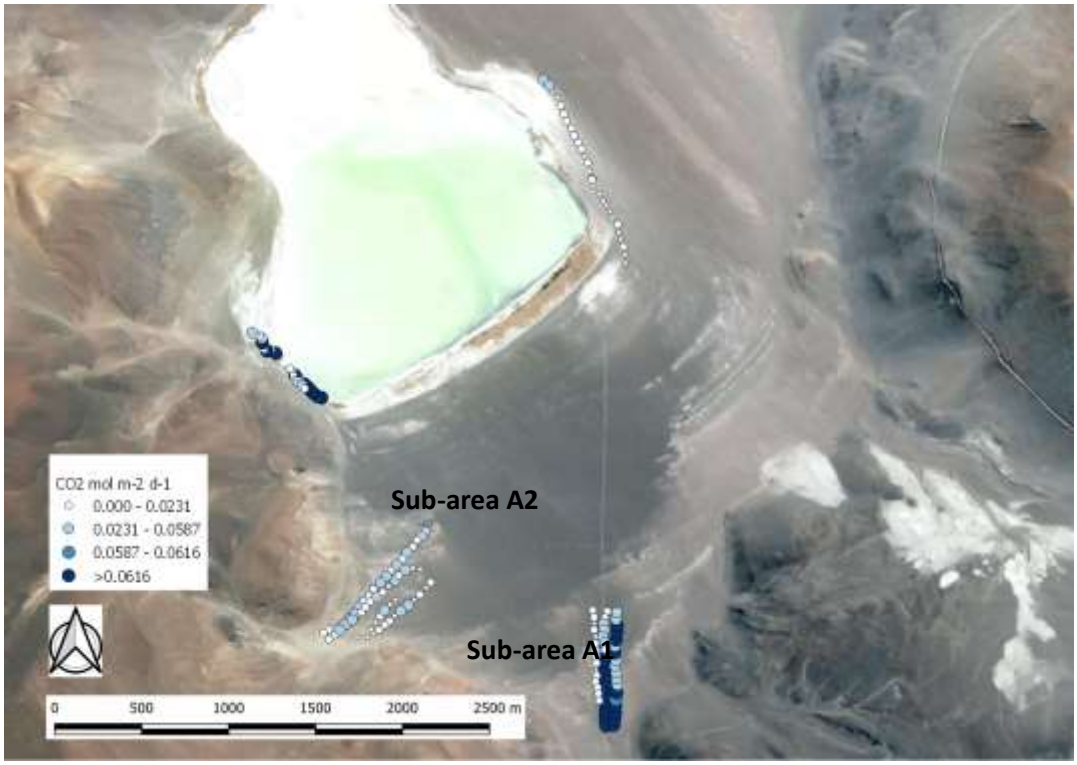

Figure 12b. Geographical distribution of the three different populations for each investigated sub-area of zone A.

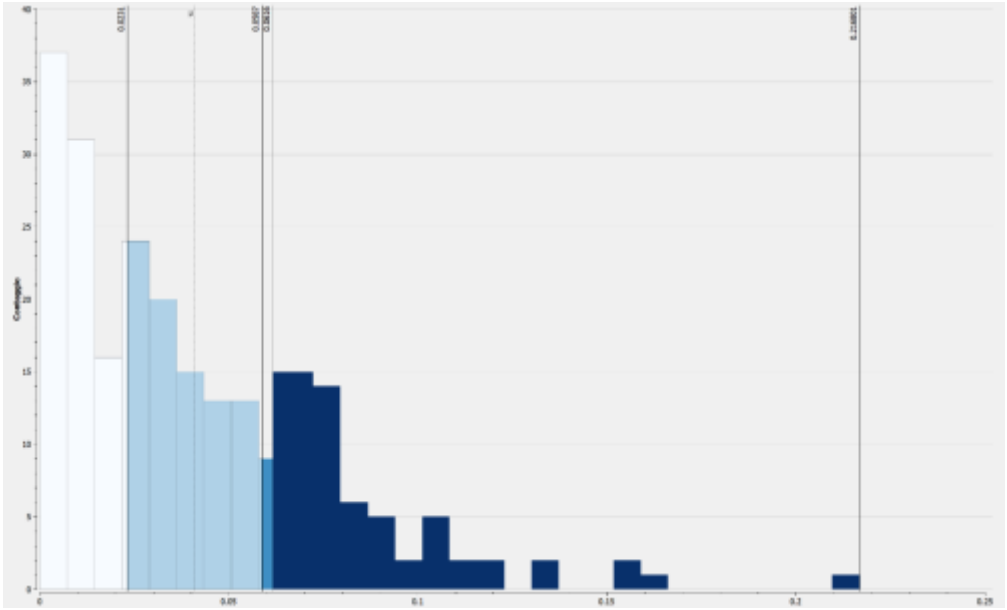

Figure 13 Histogram of the CO_2 flux value with the representation of the calculated threshold limits.

3.2 Geostatistical analysis of soil CO_2 fluxes

The geostatistical processing was performed considering only the data set related to Zone A, in particular for sub area A1 and sub area A2 (Figure 12). The adopted procedure is aimed at both elaborating an iso-CO_2 flux map.

The geostatistical data elaboration has been performed by considering no-transformed data, the omni-directional experimental variogram were obtained for a lag value of 55 m, representing an

average width of the measurement step. The variogram relating to sub area A1 data shows the only presence of "nugget effet" for this reason it is not possible to construct a mathematical model representative of spatial continuity.

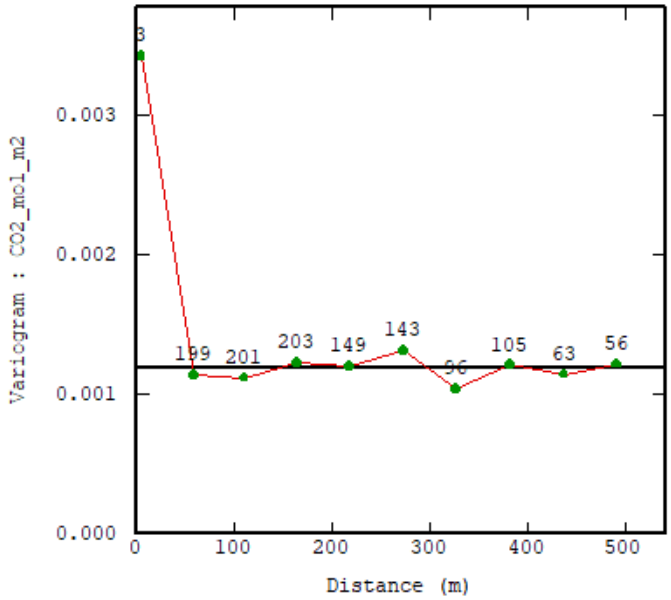

Figure 14. Omni-directional experimental variogram (red line with green dots) for the soil CO2 fluxes in the Sub Area A1. Labels close to the experimental variogram dots indicate the number of CO2 flux couples.

The same data processing has been performed for sub Area A2. The variogram is shown in Figure 15. Although only two couples represent the first point, a mathemathical modeling has been attempted by using a spherical model. The graphical results are reported in figure 15.

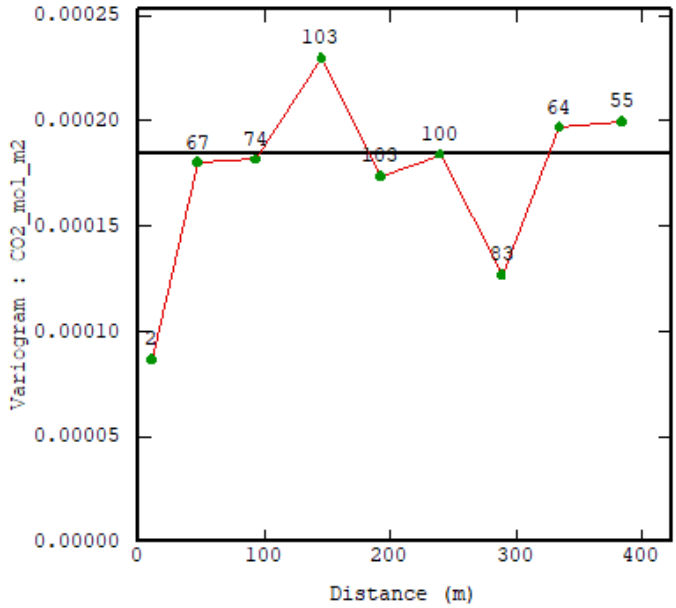

Figure 15. Omni-directional experimental variogram (red line with green dots) for the soil CO2 fluxes in the Sub Area A2. Labels close to the experimental variogram dots indicate the number of CO2 flux couples.

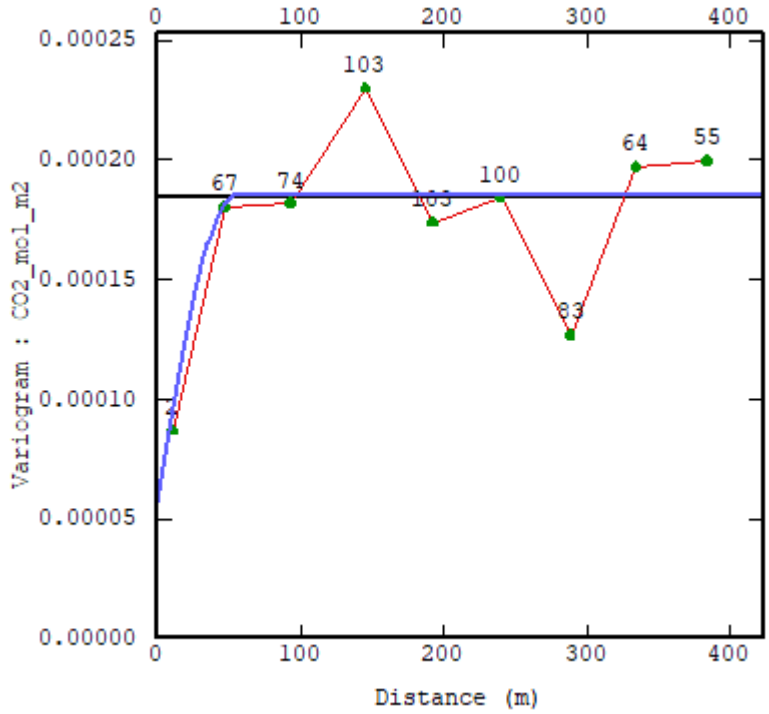

Figure 16. Omni-directional experimental variogram (red line with green dots) and fitted variogram model (blue line) for the soil CO_2 fluxes in the sub area A2. Labels close to the experimental variogram dots indicate the number of CO_2 flux couples driving each point.

The reliability of the mathematical model was tested by cross validation, a procedure that uses the variogram model to re-calculate each measurement. The results of this procedure are shown in Cross-validation diagrams. Comparison between estimated and measured values shows that model is unfit to describe the spatial variability of the system. This is in agreement with the experimental variogram that excluding the first point shows the presence of only “nugget effect”.

Figure 17. Cross validation diagrams for the variogram model of soil CO_2 fluxes in sub area A2. Green circles identify the measurements for which the difference between measured and computed values exceeds 2.5 σ.

4. Conclusion

The CO_2 flux were processed by partitioning the cumulative population of the Q-Q plot, by adopting the Sinclair's approach. This method, since the groundbreaking study of Chiodini et al. (1998), was adopted in different geothermal areas worldwide and was therefore thoroughly tested. Nevertheless, the distinction between background-biogenic CO_2 and deep CO_2 has an inherent uncertainty. The local background threshold of soil CO_2 fluxes obtained for the Socompa Volcano area is about 0.06 $mol \cdot m^{-2} \cdot d^{-1}$. This value is in good agreement with 0.05 $mol \cdot m^{-2} \cdot d^{-1}$ evaluated for Cerro Pabellón area (Taussi, 2018, personal communication) and with 0.05 reported by Raich & Schlesinge (1992) and referred to desert scrubs (located in the Federal States of Utah and New Mexico, US).

Measurements exceed the background threshold are probably linked to the presence of a more intense radical activity or, again, at different weather conditions. A deep source contribution appear to be quite improbably, this implies that this contribution is negligible. This can be due essentially to two reasons: the deep source does not exist; the impervious cover is so efficient that the flow of gas does not pass through.

References

Armstrong, M., 1984a. Problems with universal Kriging. Math. Geol., 16(1): 101-108.

Armstrong, M., 1984b. Problems with universal Kriging. Math. Geol., 16(3): 305-316.

Chauvet P., (1982) The variogram cloud, Johnson TB & Barnes RJ (Ed.) 17th APCOM, Society of Mining Engineers, New York, 757 – 764.

Chauvet P. (1991) Aide mémoire de géostatique linéeaire, Chaiers de Géostatistique, Fascicule 2. Ecole des Mines de Paris, Fontainebleau, 210 pagg.

Chauvet P. (1993) Processing data with a spatial support: geostatistics and its method, Chaiers de Géostatique, Facicule n. 4, Ecole des Mines de Paris, Fontainebleau, 57 pagg.

Chauvet P., Galli A. (1982) Universal Kriging, Pubblication n. C – 96, Centre de Géostatique, Ecole des Mines de Paris, Fontainebleau.

Chiodini G., Cioni R., Guidi M., Marini L., Raco B. (1998). Soil CO2 flux measurements in volcanic and geothermal areas. Applied Geochemistry, 13, 543-552.

Clark I. (1979). Practical Geostatistics. Department of Mineral Resources Engineering, Royal School of Mines, Imperial College of Science and Technology, London, 129p.

David M., 1977. Geostatistical Ore Reserve Estimation, Elsevier Sci., New York. 364.

Devijver, P. A., and J. Kittler, (1982) Pattern Recognition: A Statistical Approach. Prentice-Hall, London, 1982

Krige D.G., (1951) A statistical approach to some basic mine valuation problems on the Witwatersrand. J. Chem. Metall. Min. Soc. S. Afr., 52:119-139

Matheron G. (1962) Traité de géostatistique appliquée. Mémoire du BRGM 14, Ecole des Mines de Paris, Fontainebleau.

Matheron G. (1965) Les variables régionalisées et leur estimation: une application de la théorie des fonctions aléatoires aux sciences de la nature. Paris, Masson. 306 p.

Matheron G. (1969) Le krigeage universel. Les cahiers du CMM de Fontainebleau, Fasc. 1, Ecole des Mines de Paris.

Matheron G. (1970) The theory of regionalized variables and its applications, Fascicule n. 5, Les Cahiers du Centre De Morphologie Mathématique, Ecole des Mines de Paris, Fontainebleau, 211.

Matheron G., Monget J.M. (1969) Théorie des variables régionalisées. C-46, Ecole des Mines de Paris.

Parkinson K.J. (1981). An improved method for measuring soil respiration in the field. J. Appl. Ecology, 18, 221-228.

Pinault J.-L. and J.-C. Baubron, Signal processing of soil gas radon, atmospheric pressure, moisture, and soil temperature data: A new approach for radon concentration modeling, J. Geophys. Res., 101, 3157-3171, 1996.

Raich J.W. & Schlesinge W.H.(1992). The global carbon dioxide flux in soil respiration and its relationship to vegetation and climate. Tellus,44B, 81-99.

Sichel H.S. (1966) The estimation of means and associated confidence limits for small samples for lognormal population. Proc. 1966 Symp. South African Institute of Mining and Metallurgy

Sinclair A.J. (1974) Selection of thresold values in geochimical data using probability graphs. Journal of Geochemical Explorat., 3:129 – 149

Sinclair A.J. (1991) A fundamental approach to threshold estimation in exploration geochemistry: probability plots revisited. Journal of Geochemical Explorat., 41:1 – 22

Singh, A. (1993) Omnibus Robust Procedures for Assessment of Multivariate Normality and Detection Of Multivariate Outliers. In Multivariate Environmental Statistics, Patil G.P. and Rao, C.R., Editors, pp. 445-488. Elsevier science Publishers

Singh, A. K., Singh, Anita, and Engelhardt, M., "The Lognormal Distribution in Environmental Applications," EPA/600/R-97/006, December 1997.